



Long-term spectral study of the black hole Cygnus X-1 using INTEGRAL

F. Cangemi¹, T. Beuchert², T. Siegert³, V. Grinberg⁴, J. Wilms⁵, J. Rodriguez¹,
I. Kreykenbohm⁵, P. Laurent⁶, and K. Pottschmidt^{7,8}

¹ CEA/AIM Paris Saclay, 91191 Gif sur Yvette, France

² API/UVA, Science Park 904, 1098 XH Amsterdam, The Netherlands

³ CASS/UCSD, 9500 Gilman Drive, La Jolla, CA 92093, USA

⁴ IAAT, Universität Tübingen, Sand 1, 72076 Tübingen, Germany

⁵ Dr. Remeis Sternwarte & ECAP, FAU, Sternwartstr. 7, 96049 Bamberg, Germany

⁶ Laboratoire APC, UMR 7164, CEA/CNRS/Université Paris Diderot, 75013 Paris, France

⁷ NASA Goddard Space Flight Center, Greenbelt, MD 20771, USA

⁸ University of Maryland, Baltimore County, Baltimore, MD 21250, USA

Abstract. We utilize the joint capabilities of IBIS and SPI to perform a state-resolved 20–2000 keV analysis of the microquasar Cygnus X-1. In both LHS and HSS, the spectral analysis reveals the presence of a high-energy tail above 400 keV in addition to a standard, Compton-like continuum in the 20–400 keV range. We study the polarisation properties of the hard X-ray radiation, as well as of the polarisation of this high-energy tail. Polarisation is detected in the LHS in agreement with previous work. We find potential variations of the LHS polarisation with time and no polarisation detection in the HSS.

Key words. Cygnus X-1, X-rays binaries, INTEGRAL

1. Introduction

X-ray binaries show two main spectral states: the “Low Hard State”, LHS, dominated by hard X-rays and the “High Soft State”, HSS, dominated by soft X-rays. The LHS spectrum can be described by a hard power law (photon index $\Gamma < 2$) with an exponential cutoff around 100 keV, which indicates a dominance of inverse Compton scattering of a hot plasma off a lower-energy photon field. The HSS spectrum is well modelled by a steeper power law ($\Gamma > 2.5$) together with a black body like spectrum which describes an optically thick accretion disc close to the black hole. In the radio

domain, jets have been observed in the LHS (e.g. Corbel et al. 2013), but they seem absent or quenched in the HSS. The transition from the LHS to the HSS is accompanied with discrete ejections at relativistic velocities (e.g. Mirabel 1998; Rodriguez et al. 2008).

Beyond this, a high-energy tail from 400 keV up to several MeV has been detected in multiple sources (Grove et al. 1998). In Cyg X-1, it was first seen by CGRO/COMPTEL (McConnell et al. 2000), later confirmed with INTEGRAL (Cadolle Bel et al. 2006; Jourdain et al. 2012a,b; Laurent et al. 2011; Rodriguez et al. 2015, hereafter L11, R15 for the last two). In HSS, further ob-

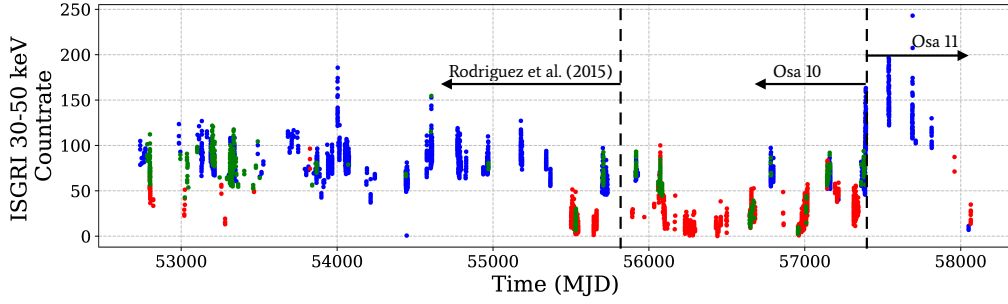


Fig. 1. ISGRI ScW-wise 30–50 keV light curve. The LHS, HSS and IS ScW are represented in blue, red and green respectively. The arrows indicate the OSA change and data used previously.

servations are needed to confirm the tail. The origin of the tail is debated; possible interpretations are synchrotron emission from the jets, or a hybrid thermal/non-thermal corona.

Here, we extend earlier work presented in L11 and R15. We gathered 15 years of data with INTEGRAL and took advantage of the source changing into HSS around 2012 and remaining in that state for considerable time. We exploit the joint capabilities of IBIS and SPI to constraint the high-energy tail in the LHS and, for the first time, collect enough data to investigate the spectrum >400 keV in the HSS. Using the Compton mode, we can use polarisation as an independent diagnostic to characterise the origin of the high energy component.

2. Observations and long-term behaviour

We consider all INTEGRAL data from MJD 52722–58064. The details of the data reduction will be given in Cangemi et al. (in prep). Since the OSA software has been updated to its 11.0 version in October 2018, which is only valid for data taken after MJD 57388, the ISGRI extraction has to be divided in two parts, see Fig. 1. We used the method of Grinberg et al. (2013) to classify each Science Window (ScW) into LHS, intermediate state (IS) and HSS.

Fig. 1 shows the long-term ISGRI light curve. Cyg X-1 mostly remained in LHS until MJD 55700 and transited on MJD 55786 into a ~ 4 years long HSS. It transited back in the LHS around MJD 57531.

We stacked individual ScW depending on their assigned state and the OSA version used due to inconsistent calibration between OSA 10.2 and OSA 11.0.

3. Phenomenological spectral analysis

The ISGRI spectra were modelled in the 25–400 keV (OSA 10.2) and 30–400 keV (OSA 11.0) range and the SPI spectra in the 25–2000 keV ranges.

LHS. We first restricted our analysis to energies below 400 keV. With `const*cutoffpl`, we obtained an adequate fit ($113.5/89 \chi^2/\text{dof}$) with a photon index of $\Gamma_{\text{cut}}=1.50\pm 0.02$ and an exponential cutoff of $E_{\text{cut}}=157\pm 5$ keV. An extra reflection component is statistically not required. We then added the data above 400 keV and froze Γ_{cut} . We do confirm hard X-ray excess emission as previously reported by L11, R15. This high-energy tail component is well described with a power law with $\Gamma_{\text{po}}=1.5^{+0.3}_{-0.5}$. Once again, no reflection is needed ($147.7/98$ for `const*reflect(cutoffpl+po)` versus $147.83/97 \chi^2/\text{dof}$ for `const*(cutoffpl+po)`).

HSS. Compared to previous studies, the larger amount of data for the HSS allows us to claim a significant excess at high energies. Below 400 keV, we started first with a simple power-law model (`const*powerlaw`) to investigate a possible cutoff, which did not describe the observation well ($275.34/52$ dof). We thus used two alternative approaches:

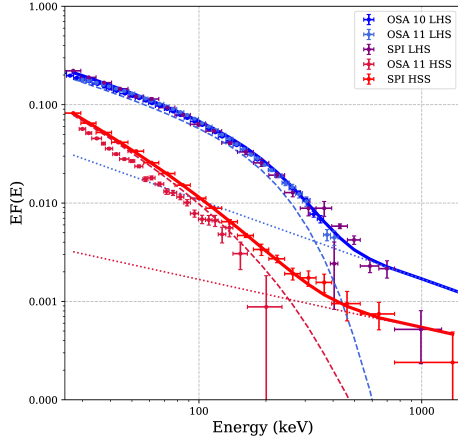


Fig. 2. Spectral results. LHS shown in blue and HSS in red. For both, we show the semi-physical model (*Model 2*) for the HSS in thick lines. The Comptonisation and power law component are represented in dashed and dotted lines, respectively.

Model 1) Add reflection, which improved the fit significantly ($148.2/51 \chi^2/\text{dof}$). We found $\Gamma=2.38\pm 0.02$ and a reflection component of $\Omega/2\pi=0.81^{+0.18}_{-0.16}$. We froze the values of Γ and $\Omega/2\pi$ and added the data above 400 keV resulting in $160.8/62 \chi^2/\text{dof}$. Letting Γ and/or $\Omega/2\pi$ free did not improve the fit.

Model 2) Using a cutoff power law instead of a simple power law ($115.5/51 \chi^2/\text{dof}$), we found $\Gamma_{\text{cut}}=2.27\pm 0.03$ with an exponential cutoff $E_{\text{cut}}=231^{+40}_{-31}$ keV. When adding data above 400 keV, we observe significant excess emission above the just described model with $135.7/62 \chi^2/\text{dof}$. Therefore, we added a high-energy power law component:

- Γ_{cut} and E_{cut} frozen: $123.2/60 \chi^2/\text{dof}$ with $\Gamma_{\text{po}}=0.094^{+0.5}_{-0.8}$
- Γ_{cut} frozen and E_{cut} free: $120.4/59 \chi^2/\text{dof}$ with $\Gamma_{\text{po}}=0.54^{+2}_{-0.8}$, $E_{\text{cut}}=223^{+16}_{-38}$ keV
- Γ_{cut} and E_{cut} free: $114.7/58 \chi^2/\text{dof}$ with $\Gamma_{\text{po}}=1.5^{+0.9}_{-0.4}$, $E_{\text{cut}}=135^{+54}_{-42}$ keV

Reflection components do not improve these fits. We prefer the *model 2*) with Γ_{cut} and E_{cut} are left free to vary from a statistical point of view.

4. Semi-physical spectral analysis

LHS. Starting from the phenomenological model, we replaced `cutoffpl` by a Comptonisation model (`comptt`). When freezing Γ_{po} from the phenomenological approach, we found $kT=55\pm 2$ keV and $\tau=0.95\pm 0.05$ ($215.9/98 \chi^2/\text{dof}$). The statistics are improved when fitting Γ_{po} freely. We found $\Gamma=1.8\pm 0.1$, $kT=51\pm 3$ keV and $\tau=1.05^{+0.1}_{-0.08}$ ($205.7/97 \chi^2/\text{dof}$). The values of the Comptonisation parameter y are compatible (0.39 ± 0.03 and $y=0.44\pm 0.06$ for Γ fixed and free). Adding reflection while freezing τ improved the fitting ($191.3/97 \chi^2/\text{dof}$), we found $\Omega/2\pi=0.23^{+0.13}_{-0.11}$, $kT=55\pm 3$ keV and $\Gamma_{\text{po}}=1.7^{+0.1}_{-0.2}$.

HSS. Starting from *Model 1*), we froze the reflection component and replaced the power law by the `comptt` model. We obtained $326.0/59 \chi^2/\text{dof}$ and thus let the reflection component free. We found $\Omega/2\pi=0.13^{+0.15}_{-0.13}$ with $kT=246^{+68}_{-23}$ keV and $\tau=0.018^{+0.03}_{-0.004}$ and a better statistic of $133.4/59 \chi^2/\text{dof}$. Then we froze τ and added a power law component to model the high-energy excess. This improved the fit ($124.7/58 \chi^2/\text{dof}$), and we found $\Gamma=-0.3\pm 1.1$ with $kT=246\pm 7$ keV and $\Omega/2\pi=0.15^{+0.11}_{-0.10}$.

Starting from *Model 2*), we replaced the cutoff power law component by a Comptonisation component. By fixing the photon index to the value found in the first approach, we found: $113.7/60 \chi^2/\text{dof}$ and $kT=78\pm 14$ keV, $\tau=0.21^{+0.08}_{-0.05}$. Freeing Γ_{po} provides the same spectral parameters.

5. Polarimetry analysis

We note that the following analysis is preliminary. We carry out the polarisation analysis using the Compton mode (Forot et al. 2007). We first analysed the full 400–2000 keV data for LHS and HSS to investigate the global polarisation of the high-energy tail. For the LHS, we detected polarisation with a polarisation angle of $40\pm 12^\circ$ and a polarisation fraction of $40\pm 15\%$. Our results are compatible with L11 and R15 but better constrained. The polarisation angle is consistent with the result from SPI, but our polarisation fraction is significantly lower (Jourdain et al. (2012b) found

$PA=40\pm 3^\circ$ and $PF>75\%$). For the HSS, no polarisation is detected with an upper limit of 51%.

Since the high-energy tail is variable (e.g. R15), we divided the whole data set into six different epochs of 932 days each and measured polarisation for each of these six epochs in a state-resolved manner. We found that the first and third epoch, both in LHS, between MJD 52722–53553 and MJD 54575–56439, respectively, are polarized. These results, however, have to be consolidated before we can conclude to an intrinsic variation of the polarisation. If confirmed, these variations could explain the somewhat lower polarisation fraction we measure.

6. Conclusion and discussion

We performed a broad-band spectral study for the LHS and HSS using IBIS and SPI. Besides the LHS, we for the first time report a firm detection of a hard tail in the HSS (see Jourdain et al. (2014) for a previous attempt). The systematics result in a large range of $\Gamma_{po} = 1.2$ – 1.9 for the LHS and $\Gamma_{po} = -1.4$ – 2.4 for the HSS. Given the data, the HSS seems to statistically indicate a lower value of Γ_{po} . We abstain from providing a firm physical interpretation of these results at this stage of the analysis, especially given the phenomenological description of the hard tail, and systematics arising when averaging over multiple source activity periods.

Using the Compton mode, we measured polarisation of the high-energy tail for both states. The tail is polarised in the LHS with hints of variability of the polarisation fraction over time. Polarisation is not detected in the HSS with 51% upper limit.

For the LHS, our results on the polarisation properties are compatible with the scenario of synchrotron emission from the jets as proposed by L11, (Zdziarski et al. 2012), R15. For the HSS, assuming that there are still jets but fainter than in the LHS (e.g. Drappeau et al. 2017), the synchrotron tail would be undetectable in the X-ray domain. Alternatively, the hard tail in the HSS could be explained by non-thermal Comptonisation; Romero et al. (2014)

predicted a fraction of polarisation of 54% in state with absence of jets which is roughly compatible with our upper limit of 51%.

The presented results are intermediate and part of a work in progress. We will in particular employ more physical models and consolidate the polarisation analysis. We will also consult radio data as a tool to connect polarisation variability to jet emission.

Acknowledgements. FC, JR, & PL acknowledge partial funding from the French Space Agency (CNES). TS is supported by the German Research Society (DFG-Forschungstipendium SI 2502/1-1). VG is supported through the Margarete von Wrangell fellowship by the ESF and MWK Baden-Württemberg

References

- Cadolle Bel, M., Sizun, P., Goldwurm, A., et al. 2006, *A&A*, 446, 591
- Corbel, S., Aussel, H., Broderick, J. W., et al. 2013, *MNRAS*, 431, L107
- Drappeau, S., Malzac, J., Coriat, M., et al. 2017, *MNRAS*, 466, 4272
- Forot, M., Laurent, P., Lebrun, F., & Limousin, O. 2007, *ApJ*, 668, 1259
- Grinberg, V., Hell, N., Pottschmidt, K., et al. 2013, *A&A*, 554, A88
- Grove, J. E., Johnson, W. N., Kroeger, R. A., et al. 1998, *ApJ*, 500, 899
- Jourdain, E., Roques, J. P., & Chauvin, M. 2014, *ApJ*, 789, 26
- Jourdain, E., Roques, J. P., Chauvin, M., & Clark, D. J. 2012a, *ApJ*, 761, 27
- Jourdain, E., Roques, J. P., & Malzac, J. 2012b, *ApJ*, 744, 64
- Laurent, P., Rodriguez, J., Wilms, J., et al. 2011, *Science*, 332, 438
- McConnell, M. L., Ryan, J. M., Collmar, W., et al. 2000, *ApJ*, 543, 928
- Mirabel, I. F. 1998, 392, 4
- Rodriguez, J., Grinberg, V., Laurent, P., et al. 2015, *ApJ*, 807, 17
- Rodriguez, J., Shaw, S. E., Hannikainen, D. C., et al. 2008, *ApJ*, 675, 1449
- Romero, G. E., Vieyro, F. L., & Chaty, S. 2014, *A&A*, 562, L7
- Zdziarski, A. A., Lubiński, P., & Sikora, M. 2012, *MNRAS*, 423, 663